Mobile Manipulation of a Laser-induced Breakdown Spectrometer for Planetary Exploration

Mobile Manipulation of a Laser-induced Breakdown Spectrometer for Planetary Exploration

Peter Lehner, Ryo Sakagami, Wout Boerdijk, Andreas Dömel, Maximilian Durner, Giacomo Franchini, Andre Prince, Kristin Lakatos, David Lennart Risch, Lukas Meyer, Bernhard Vodermayer, Enrico Dietz, Sven Frohmann, Fabian Seel, Susanne Schröder, Heinz-Wilhelm Hübers, Alin Albu-Schäffer, Armin Wedler

Mobile Manipulation of a Laser-induced Breakdown Spectrometer for Planetary Exploration

Peter Lehner[1], Ryo Sakagami[1], Wout Boerdijk[1], Andreas Dömel[1], Maximilian Durner[1], Giacomo Franchini[1], Andre Prince[1], Kristin Lakatos[1], David Lennart Risch[1], Lukas Meyer[1], Bernhard Vodermayer[1], Enrico Dietz[2], Sven Frohmann[2], Fabian Seel[2], Susanne Schröder[2], Heinz-Wilhelm Hübers[2], Alin Albu-Schäffer[1], Armin Wedler[1]

[1]German Aerospace Center (DLR)
Institute of Robotics and Mechatronics
Münchner Str. 20, 82234 Weßling,
Germany
Contact: Peter.Lehner@dlr.de

[2]German Aerospace Center (DLR)
Institute of Optical Sensor Systems
Rutherfordstrasse 2, 12489 Berlin,
Germany
Contact: Susanne.Schroeder@dlr.de

Abstract

Laser-induced Breakdown Spectroscopy (LIBS) is an established analytical technique to measure the elemental composition of rocks and other matter on the Martian surface. We propose an autonomous in-contact sampling method based on an attachable LIBS instrument, designed to measure the composition of samples on the surface of planets and moons. The spectrometer module is picked up by our Lightweight Rover Unit (LRU) at the landing site and transported to the sampling location, where the manipulator establishes a solid contact between the instrument and the sample. The rover commands the instrument to trigger the measurement, which in turn releases a laser-pulse and captures the spectrum of the resulting plasma. The in-contact deployment ensures a suitable focus distance for the spectrometer, without a focusing system that would add to the instrument's volume and weight, and allows for flexible deployment of the instrument. The autonomous software computes all necessary manipulation operations on-board the rover and requires almost no supervision from mission control. We tested the LRU and the LIBS instrument at the moon analogue test site on Mt. Etna, Sicily and successfully demonstrated multiple LIBS measurements, in which the rover automatically deployed the instrument on a rock sample, recorded a measurement and sent the data to mission control, with sufficient quality to distinguish the major elements of the recorded sample.

Contents

Figure 1: The Light Weight Rover Unit measuring a rock with the LIBS instrument at the analog test site on Mt. Etna.

1 Introduction

The analytical technique of Laser-induced Breakdown Spectroscopy (LIBS) was employed on Mars for the first time in 2012 and has since established itself as an important analytical method to investigate the elemental composition of rocks and soil on the Martian surface [1][2][3]. LIBS is also proposed for in-situ geomaterial analysis of other celestial bodies such as the Moon [4]. Both ChemCam [1][2] and SuperCam [5][6] apply LIBS to analyze the composition of Martian rocks and soils. The instruments are installed on the masts of NASA's latest Mars rovers to allow for remote sampling up to several meters.

We propose an in-contact sampling method based on a self-contained LIBS instrument module that can be picked up and used by an autonomous rover. The modular payload design allows the rover to be light by design, since not all instruments need to be installed on the system during the mission start. The payload modules can be transported to the target location with a separate spacecraft to distribute the weight, or to send a new instrument during the mission: either to recover from a fault or to update the hardware to react to new scientific findings. Furthermore, in a team of robotic systems, modularized instruments can be shared at a central location to increase productivity.

The LIBS module is picked up by the Lightweight Rover Unit (LRU), our planetary exploration rover prototype [7], at the landing site and transported to the sampling location. Once in place, the mission team selects a particular rock of interest in a segmented image of

the camera. The rover analyses the scene using stereo cameras and computes an automatic sampling operation. The manipulator picks the LIBS module from the transport location and establishes a power and communication link. An algorithm analyzes the depth information of the camera system and proposes sampling candidates on the rock. The planner computes safe motions to the best reachable candidate position and commands the manipulator to approach the stone. An impedance controller steers the torques of the manipulator to ensure a firm contact with the sample. The rover commands the instrument to trigger the measurement, which in turn releases a laser-pulse and captures the spectrum of the resulting plasma. The data are downloaded by the rover and sent back to mission control for further analysis.

The proposed method ensures a suitable focus distance for the spectrometer without a focusing system that would add to the instruments volume and weight, and allows for flexible deployment of the instrument. Sampling is achieved by the torque-controlled manipulator, which steers the instrument into a safe and defined contact at which the instrument has a suitable focus. The manipulator planning algorithms can deploy the instrument at a variety of locations: The rover can sample rocks on the ground, walls of trenches, and reachable ceilings of caves.

Though the proposed method requires a complicated task sequence, the LRU can plan and execute all operations autonomously and requires almost no supervision from mission control. Developing space rovers with a high degree of autonomy increases the rovers exploration capabilities, productivity, robustness and cost-effectiveness [8]. The high autonomy level allows the mission team to focus on the scientifically relevant aspects of the mission, ensures operation in locations with reduced communication, and allows for fast collection of data, as few technical information is exchanged with mission control.

We tested the deployment of the LIBS instrument with the LRU at the moon analogue test site on Mt. Etna, Sicily as part of the ARCHES project [9]. In the experiments we successfully demonstrated multiple LIBS measurements, in which the rover automatically deployed the instrument on a rock sample, recorded a measurement and sent data to mission control, with sufficient quality for scientific analysis. Figure 1 shows the rover measuring a rock at the experiment site.

2 Related Work

Much work has been published on robotic manipulation in general: We limit the scope of the related work to planetary exploration systems, featuring *mobile manipulation* or *LIBS* capabilities.

2.1 Mobile manipulation for planetary exploration

The Rocky 7 Mars Rover Prototype was able to position itself in front of a rock and move the mounted two degrees-of-freedom (DoF) manipulator to contact the end-effector on a rock, guiding the reflected light along an optical fiber into the rover and capturing data from the sample [10]. The rover was able to use the on-board stereo camera system to check collisions of the manipulator with the environment.

The Mars Exploration Rovers, Spirit and Opportunity, deployed instruments with a five DoF manipulator [11]. One use case was to deploy the Athena payload, a particle X-Ray spectrometer: The spectrometer, rigidly attached to the turret of the manipulator, was brought into contact with selected rocks to detect their elemental composition [12]. The software was able to perform self-collision checking during operation of the arm with a composable set of primitives, estimating the rovers shape.

The Mars Curiosity Rover and the Mars Perserverance Rover are also equipped with a five DoF manipulator with instruments rigidly mounted on a turret [13][14]. The turret is equipped with an Alpha X-Ray Spectrometer to determine the elemental composition of samples. During sampling the manipulator places the spectrometer in contact with the rock surface, while monitoring the forces enacted on the turret with a force sensor mounted at the turret actuator - a new feature compared to the manipulators used on the Mars Exploration Rovers. Although the manipulator motions are designed and verified on ground, recent work discusses autonomous targeting features for the LIBS instruments mounted on the mast [15], as well as the development of a collision model for autonomous behavior, such as robotic arm positioning [16].

While the mentioned systems are designed to deploy spectrometers in space applications, our prototype supports complete on-board autonomy of the sampling operation. Mission control only selects a desired rock for sampling in a camera image. Based on this information, the rover can compute all necessary operations on-board the rover system and execute the relevant sequence of manipulator motions without the need for additional commands or information.

The SHERP and CREX rover prototypes are designed with a common mechatronic interface to position and assemble modular payload during a mission [17]. The Standard Interface for Robotic Manipulation of Payloads in Future Space Missions (SIROM) mounted on the SherpaTT allows to manipulate and power payload modules [18]. While the concept is similar to the concept of dockable payload modules in this work, the systems do not deploy a scientific instrument, such as a LIBS instrument. In addition our prototype features higher on-board autonomy capabilities, such as creating models of unknown rocks based on a stereo vision system and employs these models to safely compute motions for obtaining samples

with the instrument.

In our previous work we demonstrated autonomous manipulation of modular payload boxes on the analog site of Mt. Etna during the ROBEX campaign to position an array of seismographs in the field [19][20]. The work presented here, in the context of the ARCHES campaign at the same test site [9], extends these demonstration in three main areas: We upgraded the docking mechanism to supply the modular payload boxes with power, designed and integrated a LIBS instrument in the form of a payload module, and upgraded the autonomous manipulation capabilities to interact and position instruments on prior unknown objects, such as rocks.

2.2 LIBS for planetary exploration

For LIBS, a pulsed laser-beam is focused onto the material of interest, where a small plasma is created from ablated material. The light emitted by the plasma is collected and analyzed in a spectrometer to give information about the elemental composition. LIBS is particularly well suited for robotic in-situ exploration since it requires only optical access to the target and measurements can quickly be achieved.

In comparison to terrestrial ambient pressure or vacuum, the low Martian surface pressure allows for an almost ideal trade-off between a relatively high amount of ablated material and a strong excitation of the plasma resulting in high signal intensities. With the ChemCam instrument on NASA's Curiosity rover that landed on Mars in 2012, the LIBS technique had its premiere in space exploration [1][2][3]. Due to the success of ChemCam, a second LIBS instrument came to Mars in February 2021 as part of the enhanced SuperCam instrument suite [5][6] on NASA's Mars 2020 Perseverance rover. Moreover, the Chinese space agency developed a rover with a LIBS instrument on board closely inspired by the ChemCam design that landed on the Martian surface later in 2021[21]. These three currently active LIBS instruments on Mars allow for measurements in distances of up to several meters from the respective rovers with telescopic systems, however weighing about 10 kg.

LIBS was shown to work also well in the vacuum of atmosphereless bodies [22][23]. The first LIBS instrument to be employed on the Moon was on board the Pragyan rover of India's Chandrayaan-2 mission [4], but the lander failed to achieve a soft landing in September 2019. With only 1 kg this LIBS instrument was particularly lightweight with no focus system and would have measured the lunar regolith in a constant distance of 20 cm below the rover's chassis.

As can be seen from the already developed instruments, LIBS payloads for space exploration can be configured in various different ways, ranging from close-range and light-weight hardware to high-performance but rather heavy and voluminous instruments. What is of most importance is that a sufficiently high irradiance on the sample is provided to initiate the laser-induced breakdown and to produce a suitable plasma in the extraterrestrial conditions. This translates into the requirement to focus the laser to a sufficiently small area. Close-range configurations can here profit from a fixed-focus approach with long depth-of-field where no focus system is required.

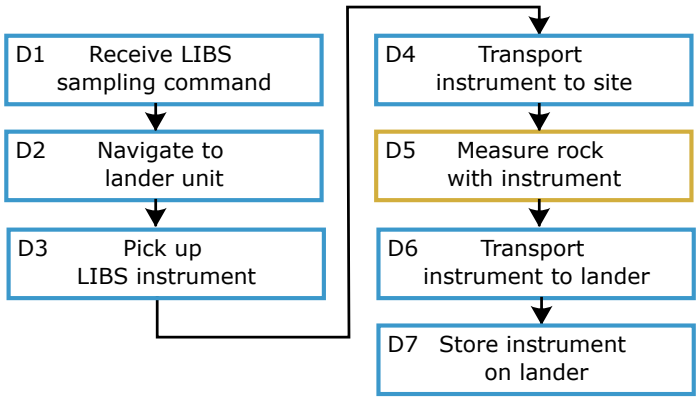

Figure 2: The complete process of deploying the LIBS instrument. This work focuses on the measurement of an individual rock with the instrument (highlighted, D5), detailed further in Figure 3

3 Overview

Autonomous in-contact LIBS sampling requires the rover to execute many individual steps, by many different components. The rover perceives the environment with cameras, reasons about the current state of the task and world, and executes the next step to reach the goal.

3.1 Manipulation Sequence

To deploy the attachable LIBS instrument the rover executes the steps indicated in Figure 2 and 3. From a high level perspective the rover needs to deploy the instrument at a target location (Figure 2). The rover first receives the LIBS sampling command with coordinates for the deployment (D1). The rover navigates to the lander unit (D2) and picks up the instrument (D3). Once the instrument is in the transport position the rover drives to the deployment site (D4), where it begins to measure rocks with the instrument (D5). After the measurements, the rover retracts the instrument and transports the payload box back to the lander (D6), where the instrument is stored until the next sampling operation (D7). While we demonstrate that the LRU can autonomously execute these operations, we focus this contribution on the manipulation aspect during the measurement (D5). For detailed explanations of the remaining navigation and manipulation operations please see our previous publications [7][20].

The process of an individual measurement of a rock is displayed in Figure 3. Once the rover arrives at the deployment location, it captures an camera image (M1) and segments individual rocks in this image: Separating the rock pixels from the rest of the image (M2). The rover transmits the image to mission control (M3), which can refine the pose of the rover, look at further images of the current scene and trigger a LIBS measurement by selecting one of the segmented rocks (M4). In communication denied environments, the rover will select the largest rock for sampling after a timeout. Once the rover receives the command

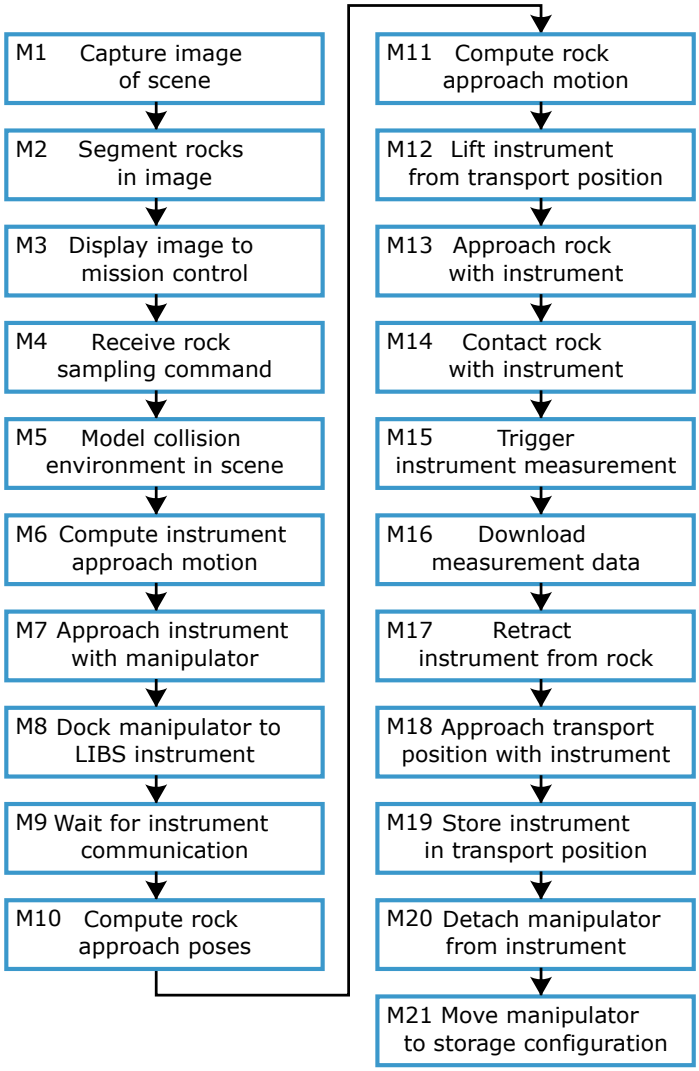

Figure 3: The manipulation process of measuring a rock with the LIBS instrument

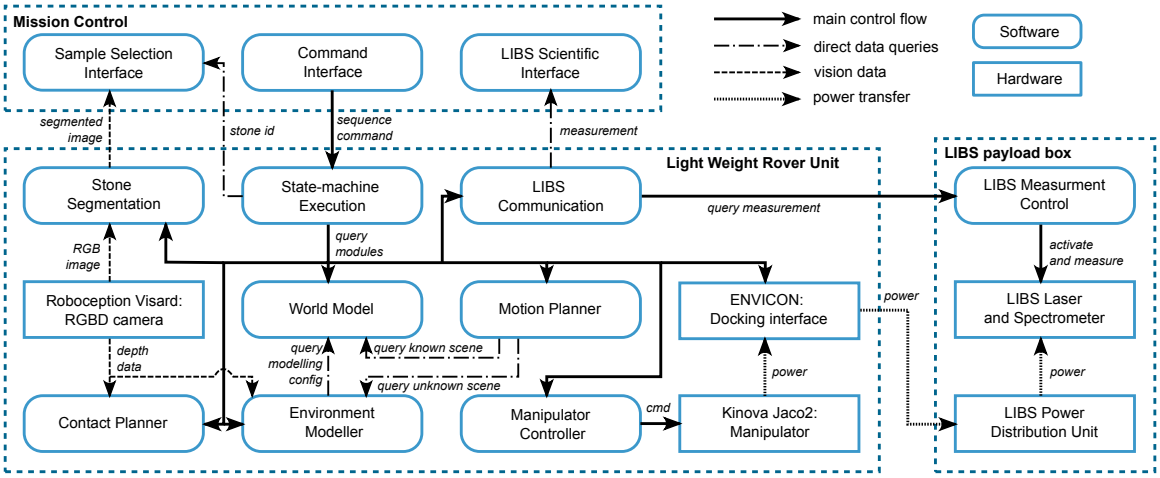

Figure 4: A hardware and software diagram of all components involved in the LIBS measurement manipulation.

to sample a rock, it first models the collision environment of the scene with the depth data of the stereo cameras (M5). To dock the instrument from the transport position to the manipulator, the algorithm computes manipulator motions for approaching the instrument (M6). The manipulator executes the motion (M7) and docks to the instrument, while controlling the contact forces (M8). Once the docking interface establishes power connection to the LIBS payload, the rover waits until it can establish a communication link with the instrument (M9).

The algorithms on the rover compute candidate approach poses on the rock surface (M10) as well as collision-free approach motions to the candidates (M11). Once a valid motion is found, the manipulator lifts the instrument from the transport position while actively controlling the contact forces (M12), and approaches the rock with the docked instrument (M13). The manipulator presses the instrument on the rock surface and actively controls the contact (M14). Once a stable contact is established, the rover signals the instrument to trigger a measurement: The instrument fires the laser-pulse and records a spectrum of the resulting plasma (M15). The resulting data is downloaded first to the rover and (if communication is established) transferred to mission control (M16). After the measurement the manipulator retracts the instrument from the rock (M17), approaches the transport position on the rover with the instrument (M18), and stores the instrument while controlling the contact forces (M19). Finally the docking interface detaches the manipulator from the instrument (M20) and the manipulator moves back into a storage configuration (M21).

3.2 Component Overview

The complete measurement sequence is computed and executed by multiple components, which are composed in the architecture shown in Figure 4. The main agents involved in the sampling operation are mission control, the LRU, as well as the LIBS payload box. Mission control commands a sampling operation through the *command interface* to the rover, sending a sequence command together with sequence specific parameters to the state-machine execution. In the case of the LIBS sequence, the additional parameters indicate the deployment site, in lander relative coordinates. Once the rover is at the deployment site, mission control selects the rock via the *sampling interface*: The rocks at the deployment site are highlighted in the current camera image and the user can select a particular rock for sampling. Once a measurement is downloaded from the instrument, mission control can quickly visualize the measurement using the *LIBS scientific interface* as fast feedback for further decisions.

Commands from mission control are sent to the *state-machine execution*, a hierarchical state-machine which orchestrates and controls the process of the individual components on the LRU. Separate from the control flow, all persistent data collected by the rover is stored in the *world model*. During the measurement the state-machine first sends a request to mission control to connect via the *sample selection interface*. The interface queries the *stone segmentation*, which in turn queries an image from the rear cameras and provides a segmented image. Once mission control selects a stone and sends the corresponding request, the state-machine queries the selected stone ID from the sample selection interface. Before computing any motions the *environment modeller* generates a model of the prior unknown part of the scene as a voxel grid, based on the depth data of the stereo cameras. The specification (region of interest) of the scene which should be modeled is stored as prior knowledge in the world model. The depth data is also analyzed by the *contact planner* to determine the places on the rock surface which are accessible for sampling. The state-machine selects the best contact candidate and queries the *motion planner* to compute safe manipulator motions. To not collide with any obstacles the motion planner queries the prior known rover environment based on CAD models from the world model and the prior unknown environment from the environment modeller. The state-machine forwards the computed motions to the *manipulator controller* which steers the *manipulator* along the desired joint path. Once the manipulator approaches a contact, the state machine switches the mode of the manipulator controller to impedance control, a control mode which actively controls the forces during contact. The *docking interface* mounted at the end-effector of the manipulator allows to establish a rigid connection to the payload box, as well as to transfer power to the instrument. Once docked, the state-machine sends commands to the LIBS payload box via the *LIBS communication* interface, which also downloads measurement data from the instrument and sends the data to the LIBS scientific interface.

The LIBS payload box receives commands to query the status of the instrument or to trigger a measurement from the LIBS communication on the rover. The *LIBS measurement control* unit receives the measurement command and activates the *LIBS laser and spectrometer* in the correct sequence, to capture the spectrum of the resulting plasma. The *LIBS*

Figure 5: The Light Weight Rover Unit (LRU) including manipulator, docking interface and payload carrier.

power distribution unit draws the power for all components on the instrument directly from the manipulator - transferred through the docking interface. The next two sections detail the individual components: Section 4 describes the hardware components while Section 5 details the software components.

4 Hardware Components

The main hardware components are the LRU, the ENVICON docking interface and the LIBS payload box. The LIBS payload box is derived as a special payload box from the general modular payload box design.

4.1 The Light Weight Rover Unit

The Lightweight Rover Unit (LRU) was first introduced in 2015 as a new type of versatile rover for mobile planetary exploration [24]. With a weight of less than 30 kg, the stereo vision system and an optimized undercarriage for driving with speeds of more than 7 $\mathrm{km\,h^{-1}}$ in rough environments, the LRU was developed as a platform for up-coming projects for planetary exploration.

For the ROBEX project [19], the LRU rover (see Figure 5) was extended by a robotic manipulator together with a docking interface and the standardized payload system was introduced. Furthermore, a second LRU was developed to perform multi robot scenarios where as the second LRU was equipped with a complex science camera module according to existing planetary rover missions.

For ARCHES project [9], the LRU rovers underwent a general technical revision and several major changes were made, to enable parts of the mission such as the LIBS experiment. An increased degree of autonomy led to an increased requirement for computational power. To this end, more modern and ruggedized processing systems based on the COM Express standard were introduced, and the design was changed to further increase the level of maintainability. The newly used 9th generation Core i7 mobile processor comprises more efficient mechanisms for throttling CPU power, resulting in more efficient usage of power. As the computational overhead is reduced according to these changes, the 200 W h rechargeable battery of the LRU can be exploited more efficiently. Further processing power was added in the form of a NVIDIA Jetson TX for extensive on-board image and navigation processing. The higher demand for energy required adaptions of the power management system.

To enable the process of manipulation of payload boxes, as well as the LIBS payload box, including the detection of stones, 3D-Vision assets were changed from single up and down view cameras to a Roboception Visard in the rear section where also the robotic manipulator is located. The broad range of wireless communication interfaces in the rover, such as high speed Wi-Fi and bluetooth, support seamless integration of external payloads into the mission planning.

4.2 Docking interface

The ENVICON docking interface for mobile robotic exploration in harsh environments was first introduced during the ROBEX campaign in 2017 [20]. The docking interface plays a key role in the process of manipulating and handling different payload systems during a range of planetary exploration mission scenarios. Furthermore, the docking interface provides power supply and data communication to a docked payload system. The key idea of the ENVICON docking interface is the capability to provide a maximum tolerance for the docking process in changing environmental properties, enabling a highly reliable mechanical and electrical connection when the target payload is docked. The docking process as described in [20] provides the transition from being highly tolerant to increase the probability for a successful docking initiation, towards being precise just before electrical and communication interfaces are connected.

During the ROBEX project, the electrical connector, that was foreseen in the original docking interface concept, could only be realized at preliminary engineering level and thus not used during the demonstration. For the ARCHES project, however, the connector part was fully developed to a mature prototype and deployed successfully during the campaign. It follows a coaxial structural concept as carried throughout the docking interface. The male part, situated in the center axis of the docking interface, carries three co-linear feathered, copper-beryllium contact rings with a diameter of 15 mm and a distance of 2 mm between each other. The female counterpart, situated in the passive coupling adapter of the payload system, is composed of three co-linear smooth brass rings in such a way that the corresponding male and female contact rings rest inside each other when the passive coupling partner is fully docked. The ground loop is closed as soon as the last contact ring

Figure 6: The ENVICON docking interface with retracted springs (lower left) and with extended springs about to dock to the payload box (right).

reaches its final position. This proposed connector principle is a basic requirement for the operation of the LIBS payload box. Apart from providing power to the LIBS payload box, the connector also accounts for safety requirements during the mission. Figure 6 shows the ENVICON as a standalone system and mounted on the LRU manipulator.

4.3 Modular payload boxes

The concept of light weight rovers for planetary exploration, specialized in navigating in harsh environments and manipulating with different tools and payloads, can be an economic approach for future planetary missions. A part of this concept foresees modular and standardized docking interfaces between the rover and different tools or payload systems [25]. This enables the rover to become a versatile multi-role asset. The set of payload systems has its origin in the ROBEX project [19], introducing the first payload box systems for the ENVICON docking interface. At that time, the mission scenario was based on an active and a passive seismographic measurement which were performed by the LRU together with a payload-box based seismograph. For ARCHES [9], several improvements were introduced: For instance, we extended the family of payload systems, enhanced the mechatronic interfaces, and standardized the electronics infrastructure.

As shown in Table 1, the available payload systems cover the range of simple variants such as sampling containers, to highly sophisticated instruments such as the LIBS payload box. The major design drivers for the LIBS payload box were: the weight limit of 2.5 kg for the complete system, the requested stabilized power supply including voltages above and below the 24 V payload bus voltage provided by the robotic manipulator, and a reliable communication interface to the robotic environment. In addition, a set of integrated sensors

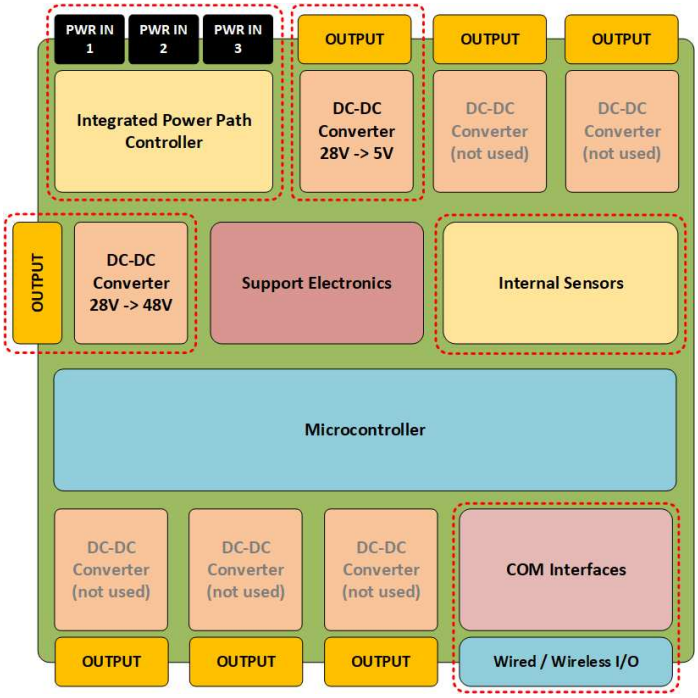

Figure 7: Schematic overview of the Payload-Box-Infrastructure-Management-System (PBIMS).

was required to meet safety requirements for the campaign.

The payload box carbon frame, intensively optimized for the ARCHES project, had to be slightly changed for the LIBS payload box. One corner of the box was trimmed so it is compatible to the manipulation and transportation tasks. The design prevented the instrument to collide to the LRU carrier structure or to the lander when in operation. This modification also allowed the laser focus point to remain within the boundary of the payload box and to accommodate the laser optics components on this newly created surface. Initially, a simple pin shaped stand-off was integrated to create a constant distance to the laser optics when the LIBS payload box was placed on a target. Later, that pin was exchanged by a cylindrical structure which was trimmed to the boundaries of the original payload box structure, showing more stability and reduction of load to the robot arm's joints during manipulation and placement on the sample target. The cylindrical stand-off also contributes to the laser-safety features, as the visibility to the laser-orifice is reduced.

Besides the passive sample payload box, each payload box is regularly equipped with a Payload-Box-Infrastructure-Management-System (PBIMS). As depicted in Figure 7, this system provides not only power to the complete system by establishing regulated power for up to seven different voltages, but it is also capable of managing up to three different input power sources. Furthermore, it comprises different on-board sensors, such as an Inertial Measurement Unit (IMU) and environmental sensors. It also has a broad spectrum of wires

Table 1: Overview on different payload boxes, derived from the standard payload box frame

Box-Type	Role	Weight [kg]
Sample-Box	Collection of stones and sands	1.3
Power-Box	Powering of functional PLBs	2.4
Repeater-Box	Wireless Network Repeater	2.2
LOFAR-Box	LOFAR Radio Telescope	2.5
NAV-Box	Precise radio based navigation	2.4
LIBS-Box	Mobile Geological Spectroscopy	2.3

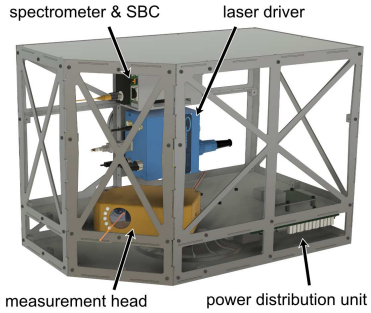

(a) CAD model of the LIBS payload box.

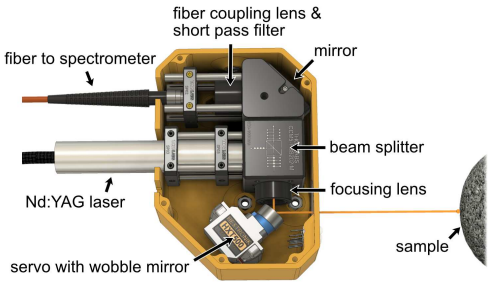

(b) CAD model of the LIBS measurement head.

and wireless communication interfaces to provide telemetry data and power bus control to the field infrastructure or the computers enclosed in the payload box. The design of the PBIMS is as compact as possible without losing the flexibility to support different types of active payload boxes. As shown in Figure 7, the LIBS payload box uses a subset of available components on the PBIMS, as only two of the seven available DC-DC converters are in use.

4.4 LIBS payload box

The LIBS payload box accommodates the measurement head, laser driver, a compact fiber coupled spectrometer, and a single board computer. These components add about 1 kg to the basic payload box and are arranged to keep the center of mass close to the docking interface which is on the backside of the box in Figure 8a. The heart of the measurement head is the q-switched Nd:YAG laser and a beam delivery optics that focuses the laser pulse on the target at a fixed distance of about 70 mm from the head (Figure 8b).

A tubular spacer (not shown) ensures correct focus distance by physical contact to the sample. The laser creates the micro-plasma with a pulse energy of about 8 mJ at 1064 nm wavelength and 5 ns pulse duration. A deflecting mirror mounted on a servo-motor in the measurement head allows to scanning the laser over the sample surface without repositioning the whole payload box. An angle of about 8 degrees between the mirror's surface normal

and the axis of rotation creates a wobble motion which results in a 3 cm long arched 1-dimensional scan on the sample surface. The same optics collect the light emitted from the laser induced plasma in backwards direction. This light is separated from the laser path via a beam divider. A short pass filter blocks the intense laser light that is scattered from the sample back into the optics but allows the relevant plasma emission to pass.

The collected light is then coupled into an optical fiber and delivered to the Avantes AvaSpec-Mini grating spectrometer. Its spectral range is 530 nm to 770 nm, which covers characteristic lines of the major rock forming elements like silicon, potassium, and calcium. The exposure time of the spectrometer is kept short at 100 µs and is synchronized to the laser pulse to minimize influences from sensor dark current and ambient light. The instrument achieves a sample rate up to 30 Hz, which allows for numerous sampling points within a short measurement time. The electrical power consumption is about 5 W in idle and about 30 W during sampling which typically takes a few seconds only. The power is delivered through the docking interface from the LRU, but could also be supplied by an additional battery within the payload box to extend action time.

To ensure safe laser operation during the ARCHES campaign on Mt. Etna, several technical features have been implemented into the LIBS payload box. The interlock switch for the laser driver is relayed to the outside of the LIBS payload box in the form of a dongle, clearly visible to the user working in the vicinity of the box. If the dongle is attached, the laser driver is active and the laser is ready to fire. An Inertial Measurement Unit (IMU), integrated into the LIBS payload box infrastructure management system is capable of constantly providing the pose of the laser orifice in order to provide firing clearance only if the beam direction is facing towards the sample on the ground. The infrastructure management system also provides the capability of shutting down the power supply to the LIBS payload box at any time. Similar to the usage of the IMU, the information regarding the positions of the robot manipulator joints are used to evaluate the pose of the robots end-effector, where the payload box is docked. Furthermore, the algorithms can evaluate the joints positions to check if the instrument is oriented towards the ground in front of the rover. Thus, the risk of unintended firing of the laser during manipulation can be significantly reduced.

5 Software Components

The autonomous capabilities of the LRU stem from the core software modules and algorithms, introduced in Section 3, and detailed in this section.

5.1 State-Machine Execution

The autonomous execution of the LIBS measurement process is managed by our open-sourced framework RAFCON [26], a framework to program and execute robotic skills as hierarchical, concurrent state machines. To complete the manipulation process, the rover

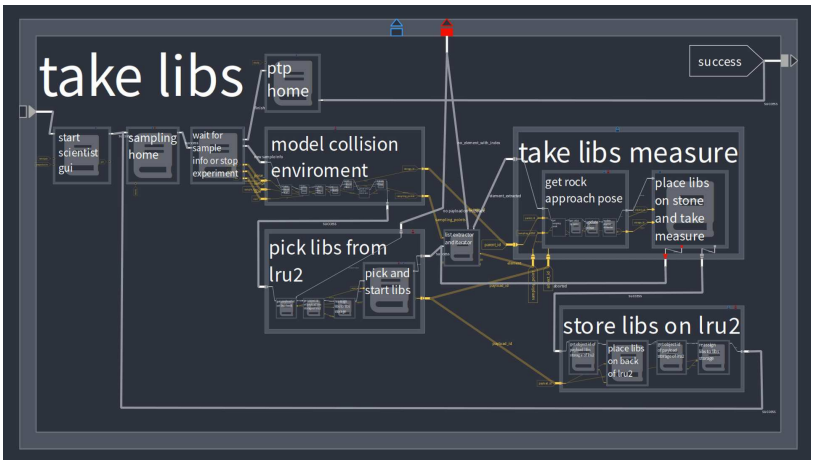

Figure 9: The RAFCON state machine of the LIBS measurement.

must orchestrate the various software components (which we call *capabilities*) by deciding which capability to trigger when, and with what parameter values. RAFCON enables users to program these complex decision-making behaviors in a hierarchical manner with a feature-rich graphical user interface (GUI). The lowest-level state machines are called *execution states* and contain a Python script, which is executed when the state-machine is triggered. The scripts mainly call the service oriented APIs of the capabilities, such as to query and update the world model, trigger the stone segmentation, and plan and control the manipulator. These execution states are connected by logical and data flows in a *hierarchical state* to implement higher-level skills. Different logical outcomes can be connected to trigger different state machines depending on conditions, which makes it possible to implement robust error-handling strategies. Easy reuse of state machines into others as *library states* leads to increased maintainability with less code duplication.

As an example of the implemented state machines, the main LIBS sampling skill (corresponding to the process in Figure 3) is shown in Figure 9. The main control flow is indicated in white connections while data flows are indicated in yellow connections. The skill is mainly composed of five major hierarchical state machines: waiting for the human inputs via the sample selection interface, modeling an collision environment, picking the LIBS instrument from the holder on the rover, taking the LIBS measurement, and storing the instrument in the transport position. The above steps are iterated until the operator is satisfied with the obtained results and continues with the next command. An example of the error handling strategies can be seen in the "take libs measure" step. If placement of the LIBS payload box on the stone fails, a different contact point of the stone, returned by the contact planner, is employed. The state machine contains 709 states with up to 10 hierarchical levels, 959 logical transitions, and 1020 data flows. Despite the complexity of the skill, the task flow is as easy to capture as shown in Fig. 3 with the intuitive support of the GUI.

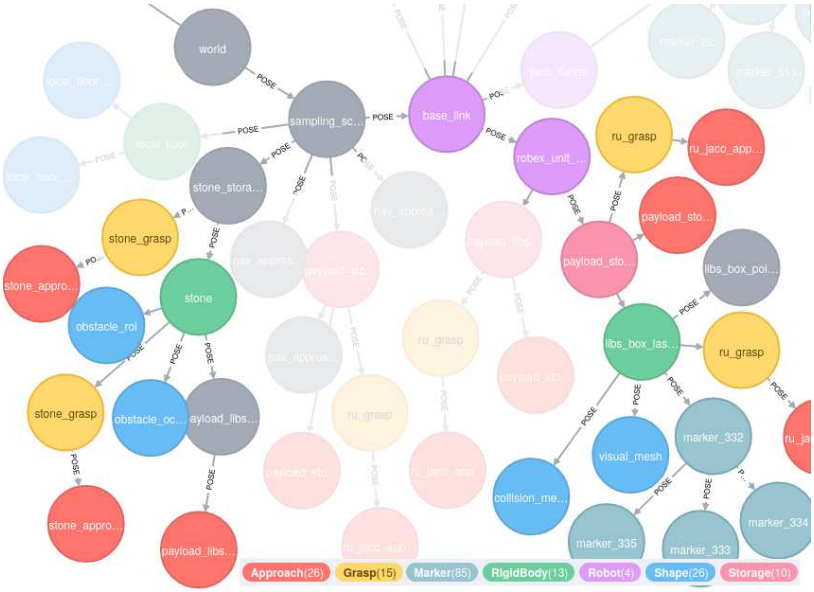

Figure 10: Tree view of the world model after modeling the stone in the scene, highlighting the sub-tree containing the stone (left) and the LIBS payload box (right).

5.2 World Model

Many components in a complex robotic system depend on information about the current environment and the state of the robot. In the context of the LIBS measurements, for example, the motion planner needs the current geometric representation of the environment, the manipulator controller needs the load data, and the object localization needs the camera position. Even though the data are heterogeneous, they are all based on the current physical situation. If the situation changes, all components must be informed of the changes accordingly. To manage this synchronization effort, we use a central representation of this data, the world model, from which the relevant aspects for the different components can be generated.

The world model consists of objects that are linked in a tree structure as shown in Figure 10. The links represent a parent-child relationship with a homogeneous transformation. The objects themselves can be physical objects, e.g. a stone or a measuring instrument (shown as green *RigidBody* nodes). But objects can also be virtual, e.g. an approach position for a grasping process (shown as red *Approach* nodes). The robot itself is also represented as objects in the world model (shown as purple *Robot* nodes). Using this simple structure, complex physical relationships can be specified at a high level of abstraction. For example, when the rover grasps an object, a new parent relationship to the robot end-effector is added to the object and the previous parent relationship of the object is removed.

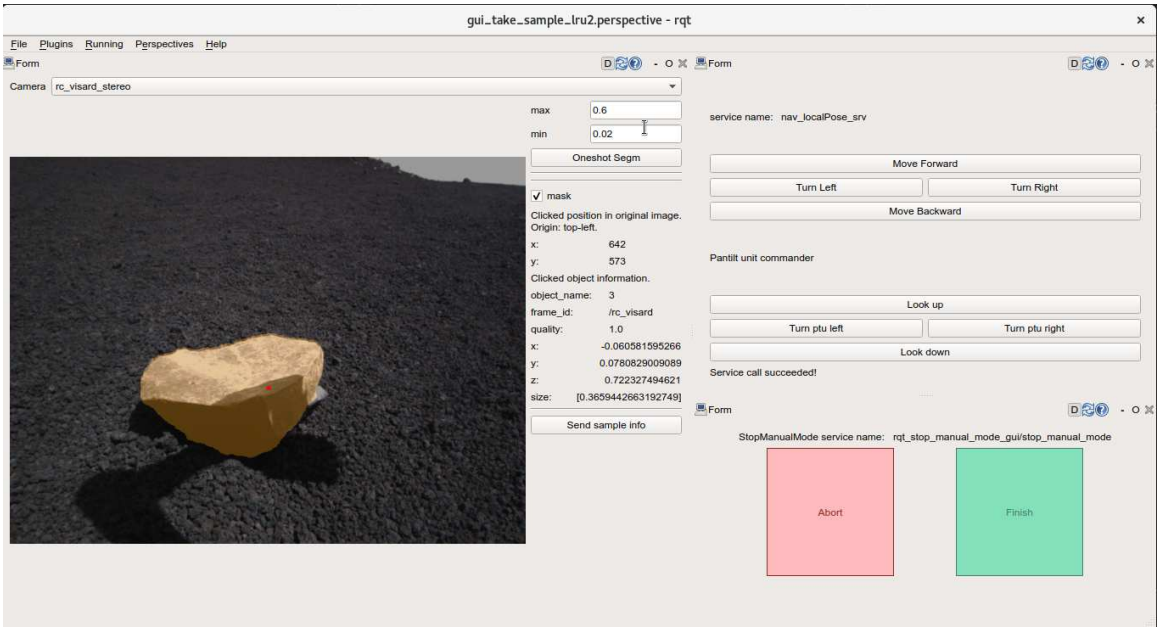

Figure 11: Screenshot of the sample selection interface.

The data is stored in the Neo4j [1] graph database. It can be accessed by different interfaces in a plug-in concept. There are interfaces which extract the geometric representation, calculate load data at the end-effector of the manipulator, or determine semantic states for decision making. These interfaces are also used to integrate newly acquired knowledge, e.g. the detection of a new object.

5.3 Stone Segmentation

To present the operator with a preview of which stones can be selected during the sampling operation as well as to infer the shape of the stones, the stone segmentation module separates stones from the background of the camera image. At the beginning of the applied perception pipeline, general knowledge about existing rocks within the field of view is generated. This information of the spatial location of the stone is required for the contact planning, and additionally aids the user experience. Therefore, we apply a learning-based object detector. Hereby, one main challenge is the almost infinite variety of natural rocks regarding shape, size, and texture. As a result, no specific 3D model to train a conventional detector can be generated. To address this issue, an unknown object segmentation technique known as Instance Stereo Transformer (INSTR) [27] is used. Rather than focusing solely on known objects, INSTR understands the concept of *objectness* and can thus detect arbitrary object instances on planar surfaces. INSTR does not require any additional fine-tuning on context-specific data, which makes it especially valuable in the planetary context where annotated

[1] https://neo4j.com/

data is particularly scarce [28]. Furthermore, by taking a stereo image pair directly as input, INSTR implicitly fuses RGB and disparity information. Hence, the method avoids the need for high-quality depth data, which can be challenging to obtain in extreme, (quasi-) extra-terrestrial environments like on Mt. Etna (e.g., lack of texture, strong solar radiation, or shadows). The resulting rock instance masks can then be further filtered by size.

5.4 Sample Selection Interface

Although the measurement steps are executed autonomously, it is quite important that the mission team can join the sample selection process with the rover. While targeted campaign sites can be strategically defined in advance, the actual geological context and the relationships between the samples, which are essential for fruitful scientific achievements [29], can be obtained only after the arrival. Therefore, the mission team is required to make a final decision on the samples most valuable for the LIBS measurements, both reactive and tactical, based on the current in-situ data. For such a decision-making, the actual scene needs to be inspected from multiple different perspectives by refining the pose of the rover with regard to the stone. Furthermore, the technical constraints must be also taken into account; only the stones detectable by the segmentation process can become the candidates of the measurements.

To satisfy these requirements, the sample selection interface was developed and utilized. Fig. 11 shows the screenshot of the GUI, which is automatically opened after the rover arrives at the targeted site. The GUI consists of the three widgets: the segmentation widget (left), the teleoperation widget (right top), and the closure widget (right bottom). With the segmentation widget, the mission team can first choose a camera to be used via the drop-down menu on top. After filling the maximum and minimum diameter of the stones to be detected, pressing the button below triggers the stone segmentation. The segmentation image is overlaid with the current image stream as an additional layer, which helps the mission team to understand which stones satisfy the technical requirements for measurements. The visualization of the layer can be controlled by toggling the checkbox below, allowing for the possibility to hide the segmentation result when not needed. The mission team is able to click the segmented area of the image to select the stone for measurements. Once the selection is confirmed by the small red dot on the clicked spot as well as the debug information, pressing the “send sample info” button at the bottom sends the stone ID, size, and pose to the running RAFCON state machine and makes it continue with the execution to take a measurement on that stone. The teleoperation widget enables the mission team to refine the rover pose relative to the targeted stone and to move the pan-tilt camera unit to look at the stone properly. The closure widget provides a way to terminate the GUI and let the rover decide how to proceed with the rest of the mission. Pressing the green button let the rover finish the LIBS measurement state machine and continue with the rest of the mission. Pressing the red button, on the other hand, aborts the current sampling operation in case of an unintended situation, for example if none of the stones are visible at the targeted site and re-positioning with autonomous navigation is needed once again.

All of the widgets are implemented as Rqt [2] plugins. Rqt is a Qt-based framework for GUI development for ROS and enables users to configure the window with any other plugins. The resulting flexibility of the sample selection interface allows further development of additional widgets if necessary.

5.5 Environment Modeller

The motion planner needs a model of the environment in order to plan collision free paths with the robot arm. But when placing the LIBS instrument on a rock, the shape of the environment is not known beforehand and the environment must be modeled online from observations. This is done based on depth images derived from stereo images by using Semi-Global Matching [30]. During the experiments we used the stereo camera mounted close to the robot arm of the LRU as they are closest to the sampling site. It is also possible to use the cameras mounted on the pan tilt unit if more flexibility is needed.

In order to generate a 3D representation from the depth image, the algorithm constructs an Octomap [31]. The model represents the world as voxels in a grid, with a 1cm resolution in our particular case. Since the manipulator is restricted to a relatively small area next to the rover, the software needs to only model the relevant space. To achieve this, a 3D bounding box of the relevant area is placed in the world model and the Octomap only models the area inside that cuboid. This reduces the size of the Octomap in memory.

By using the intrinsic and extrinsic parameters of the calibrated camera, each pixel, for which a depth value was estimated, is used to update the occupancy probabilities of the voxels in the Octomap. This also enables combining multiple images captured from different vantage points to form a single map. In this specific case only a single image is used, since the arm operates is a small and easy to observe area. If a single view is used to create a map, it is often incomplete due to objects (e.g. the rock being sampled) occluding the environment behind them. During our testing this potential issue never resulted in a collision.

To avoid updating the map while the arm is occluding the camera or while the rover is driving, the environment modeller does not run continuously. Instead, it is triggered from a RAFCON state machine just before planning a motion with the arm is started. This is also more efficient since the mapping is only performed when actually needed.

5.6 Contact Planner

To place the LIBS instrument reliably, the rover must select a suitable contact point on the selected stone. This point must fulfill two criteria: flatness and uprightness.

The flatness criteria is needed to ensure that the tubular nozzle of the instrument can rest evenly on the surface. It only applies to a small area around a candidate point (radius $r_s = 5cm$).

Uprightness means that the chosen point on the rock should be contacted with the nozzle of the LIBS box straight above it. This is motivated by hardware limitations of the

[2] http://wiki.ros.org/rqt

used robot arm, when operated in Earth's gravity. To prevent overheating due to excessive continuous torques, the manipulator can only hold the instrument for a short period of time. This issue is exacerbated by the heat on Mt. Etna. During the actual measurement most of the LIBS boxes weight rests on the stone. Placing the nozzle on a sloped spot could result in it sliding of. By using a stronger manipulator the uprightness criteria could be dropped, which would enable measurements on more surfaces, e.g. the ceiling of caves.

In order to quantify these two criteria a 3D representation of the stone is needed. The same process of creating an Octomap from depth images described in the previous section is also used as basis for the contact planner. But the area covered by the Octomap is not defined by a 3D bounding box, but instead by the 2D segmentation mask of the rock. This means that only those pixels in the depth image which are part of the stone according to the segmentation mask are integrated into the Octomap. Only locations on the stone itself are considered as candidates for the measurement. Additionally, by having fewer voxels, the following calculations are sped up.

The normal vector of a voxel is calculated in reference to the direct neighboring voxels. The normalized sum of the direction to every free neighboring voxel is the normal vector $\vec{n}$. Note that for this calculation unknown voxels (those not observed, e.g. because they are on the inside of the stone) do not count as free. We introduce an uprightness score

$$s_u = 1 - min(\frac{2}{\pi}\ arccos(\vec{n} \cdot \begin{pmatrix} 0 \\ 0 \\ 1 \end{pmatrix}), 1) \tag{1}$$

which can be directly calculated from the normal vector $\vec{n}$.

A value for flatness is calculated by iterating over every occupied voxel closer than r_s to the candidate point c. For each point p the distance

$$d = |\vec{n} \cdot (p - c)| \tag{2}$$

to a plane defined by the candidate point c and its normal vector $\vec{n}$ is calculated, the largest distance is called d_{max}.

Using that distance we define the flatness score as

$$s_f = min(1 - \frac{d_{max}}{2r_s}, 1). \tag{3}$$

These scores are combined to form a final score

$$s = min(s_u, s_f). \tag{4}$$

This score is calculated for each voxel ($1cm^3$). The voxel with the highest score is the preferred location to take a measurement. But since there are some factors not considered by this algorithm (e.g. if the manipulator can reach that contact point), ten different sampling points are generated. The resulting contact points are ordered by descending score, and the executing state-machine cycles through the candidates until a reachable contact is found.

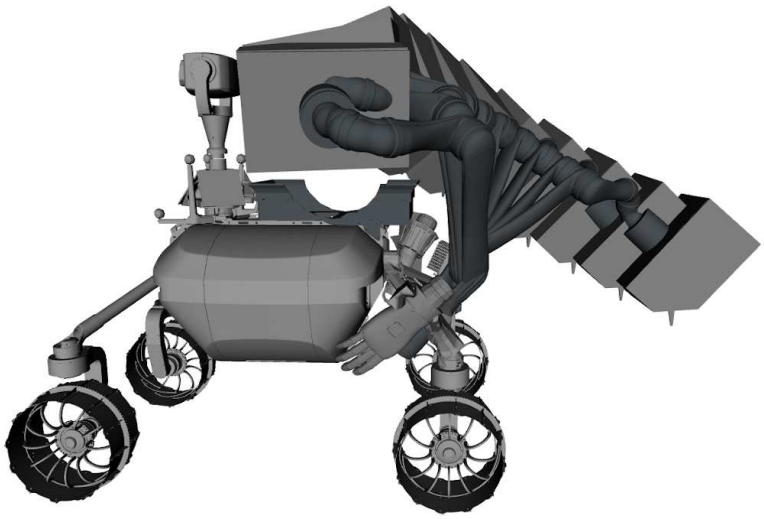

Figure 12: Manipulator motion for an approach with the LIBS instrument, computed by the motion planner.

5.7 Motion Planner

During manipulation of the payload box, any unintended contact of the manipulator with the environment might endanger the mission objective. Similarly, any collision with the rover parts might damage the instrument or one of the rover components. While executing motions, the manipulator and objects attached to the docking interface must not collide with the rover or the environment. During each LIBS sampling operation the rover computes contacts with the stones based on the input of the cameras. As a result, each operation requires different motions of the manipulator to deploy the instrument on the rock surface. The motion planner satisfies these two requirements by computing collision free motions of the manipulator, which move the docking interface to the desired target coordinates.

Computing collision free motions for the manipulator is challenging: The algorithm must find a solution path in a high dimensional search space, while respecting the non-linear kinematics of the manipulator and observing additional constraints, for example torque limits in the manipulator joints. We implemented a variant of the Rapidly-Exploring Random Tree (RRT) [32], a sampling based planning method which builds a search tree in the collision free space of the manipulator configuration space. In each iteration the algorithm samples a configuration of the manipulator and attempts to connect the tree to the new sample. We implemented the CBiRRT2 variant of the RRT planner [33], which grows two search trees: One search tree from the start configuration and one search tree from the goal. The algorithm efficiently includes additional constraints (such as joint torque constraints) with projection and rejection sampling while extending the trees. Once the algorithm finds a connection between both trees, a non-optimal solution is found. We apply a randomized shortcut algorithm to compute a local optimal solution [34]. To decrease

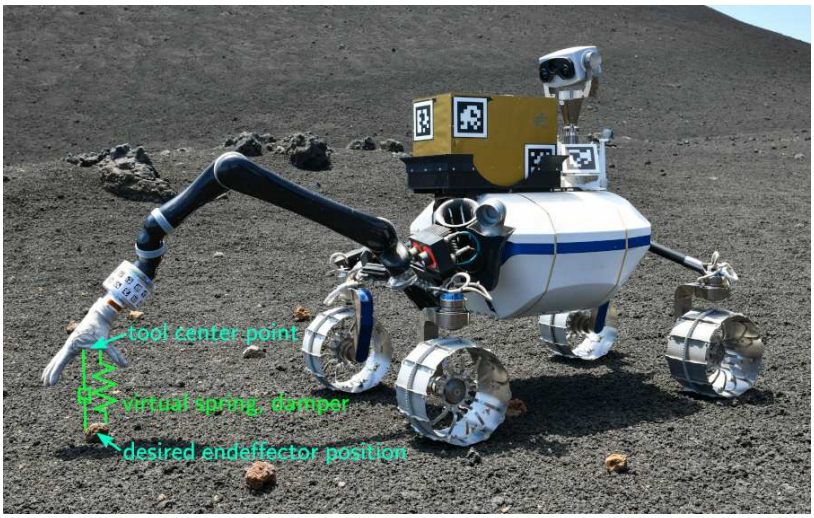

Figure 13: The LRU picking a rock with the manipulator during the ARCHES demo mission. The Cartesian impedance controller acts as a virtual spring and damper between tool center point and its desired position.

computation time, the algorithm can learn from previous solutions by guiding the tree expansion with a task specific sampling distribution [35].

To compute the collision free path the motion planner queries the current environment information from the robot world model: The transformations between the robot base to the individual objects in the scene, and a geometric representation of the object. In case of prior know objects, i.e. the LIBS instrument, the planner loads a mesh as geometric representation. Prior unknown objects, i.e. the rock and its surrounding floor, are marked in the world model and the planner queries a voxel grid representation directly from the environment modeller. The algorithm loads all geometric representations into a common scene graph and checks for collisions between the manipulator and other objects.

During the LIBS sampling operation, all approach motions are computed and verified with the motion planner as show in Figure 12: the approach of the LIBS instrument in the transport position with the docking interface, the approach of the rock with the instrument, the approach to store the instrument in the holder, and the return of the manipulator into the storage configuration. After each approach motion the state-machine switches the control mode of the manipulator into impedance control to actively control the forces during the contact.

5.8 Manipulator Controller

For the manipulation tasks performed during the ARCHES experiments, a Cartesian impedance controller was used during contact situations. The concept of impedance control was introduced in [36]. Since then, it has been extended to a wide variety of robotic applications (see

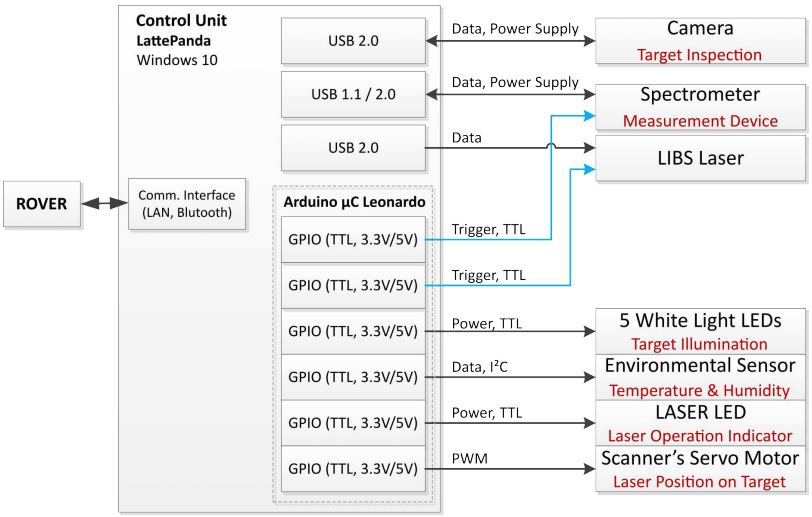

Figure 14: LIBS instrument control scheme.

e.g. [37], [38]). The Cartesian impedance controller allows to implement a desired stiffness and damping behavior w.r.t. the robot's end effector. This creates a well-defined, robust and compliant behavior in contact situations, while driving the end effector to a desired position. The concept is sketched in Figure 13. The virtual end-effector torques created by the Cartesian impedance controller are mapped to corresponding joint torque commands. Due to the aforementioned properties, the use of this control concept is indicated in situations where the manipulator moves into contact with the environment. However, the concept is also particularly useful if inaccuracies exist in the relative positioning of the tool center point and the goal position. A compliant behavior of the end effector can avoid damage of the hardware and help to fulfill the task.

5.9 LIBS Measurement Control

The LIBS measurement control is the instrument's firmware that controls all the hardware components involved and allows to perform predefined LIBS measurements and to process raw data. Figure 14 shows the instrument's hardware groups and how they are interconnected. The instrument's computer is a LattePanda miniPC running Windows 10, 32bit. The LattePanda includes an Arduino Leonardo micro-controller that is used to trigger the laser to fire and the spectrometer to acquire spectra, as well as to control the position of the laser spot on the surface of the target.

Measurements can be performed manually through commands available in the firmware, but can also be predefined and executed by the rover/user through a single command.

A measurement can consist of multiple LIBS spectra taken at a single or multiple different target positions, including dark spectra. All acquired raw data and an associated log file are stored on the internal SSD. After a measurement, the raw or processed data can be

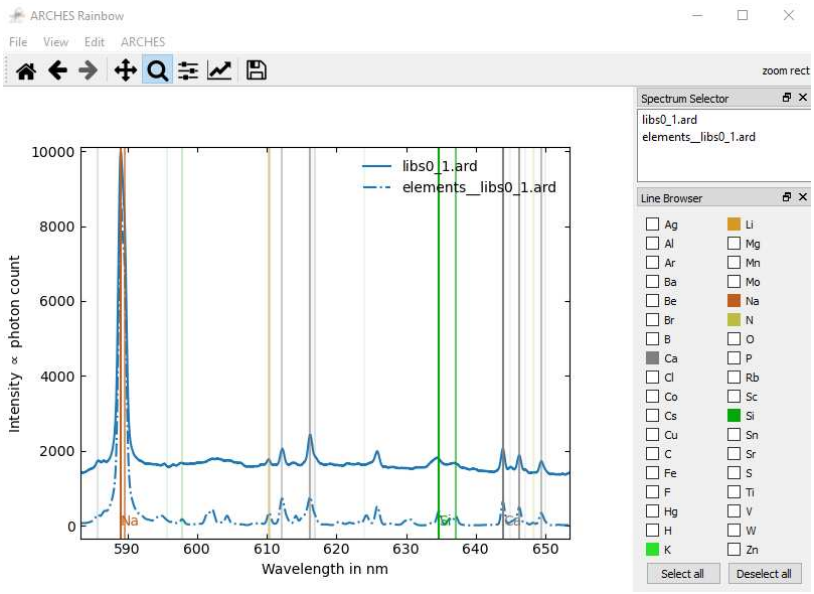

Figure 15: Screenshot of the interface for scientific LIBS-data evaluation

retrieved and transferred to the rover. Data processing includes averaging, removing the dark signal from the spectrum, and creating a preview image of a spectrum.

5.10 LIBS Scientific Interface

After the LIBS measurement procedure was executed successfully, the scientific data is received by mission control. Upon receiving the data, a custom software with a GUI displays the data for further evaluation and analysis by the participating scientists. The software was implemented in PyQt and a screenshot of the GUI is shown in Figure 15. The interface provides basic tools to the scientists that include dark spectrum removal, continuum emission removal, smoothing and different normalization methods. Measurements can be displayed as single-shot-data and as averages over several shots and locations. Multiple measurements can be compared against each other to identify changes in the sample material between different measurements. To aid the scientists in the identification of elements, a database containing the emission lines of common rock-forming elements can be used to display the position and intensity of the selected emission lines. Furthermore, the sample's elemental composition can be identified automatically. This is done by an algorithm fitting a modeled spectrum to the measured data [39]. The emission lines of the identified elements are automatically highlighted and the spectrum for each identified element can be displayed for further analysis.

6 Analog Experiments on Mt. Etna

We evaluate the LRU and LIBS instrument prototypes at an analog site on Mt. Etna, Sicily, as a proof of concept of the overall design and implementation in a relevant environment.

6.1 Experiment Site on Mt. Etna

The volcano Mt. Etna is a well known planetary analog testing site that provides an environment similar to the Moon in terms of appearance and several geological aspects [40]. Mt. Etna is frequently used for robotic tests and analog missions, for example our campaigns ROBEX [19] and ARCHES [9], or other tests that validate space exploration instruments, e.g., testing a ground penetrating radar for the ExoMars mission [41].

Our experiment site is located at approximately 2700 m altitude. It is a planar surface, positioned between the Cisternazza crater and the Monte Escrivà, one of the smaller volcanic cones located on the flank of Mt. Etna. The surrounding cone and crater limit the access to the measuring site and also block the line of sight, increasing the safety during the experiment. This is of special importance, as Mt. Etna is a highly frequented tourist attraction and potential by-standers need to be kept at a safe distance.

The experiment site mostly consists of compacted gravel with few centimeters of diameter, but additionally features sparsely scattered basaltic stones and volcanic bombs of significantly larger sizes. The scene can be seen in Figure 1. Basaltic stones with flat surfaces were selected as measurement targets, such as the one in the foreground of Figure 1.

6.2 Manipulation Sequence on Mt. Etna

On the analog site, the rover demonstrated the autonomous LIBS sampling routine, as shown in Figure 16. After mission control selected a rock in the sample selection interface, the manipulator docked to the instrument and the rover created an environment model of the stone with the back stereo cameras (a). Based on the environment model the contact planner computed the best deployment location on the stone and the motion planner computed a collision free motion to the approach (b). The manipulator executed the approach motion (c) and switched to impedance control model to prepare for contact (d). Once the desired contact was reached the rover triggered the instrument measurement, which in turn fired the laser and recorded the resulting spectrum of the plasma (e). Once the measurement was recorded and downloaded to the rover, the manipulator retracted and the motion planner computed a new motion to the back of the storage position on the rover (f). Finally the manipulator inserted the instrument back into the docking position while actively controlling the contact forces and safely released the payload (g, h). The complete sequence was executed completely autonomous based on the computations on the hardware on-board the LRU without any additional commands from mission control. The data was downloaded from the rover to mission control after the experiment and analyzed with the LIBS scientific interface.

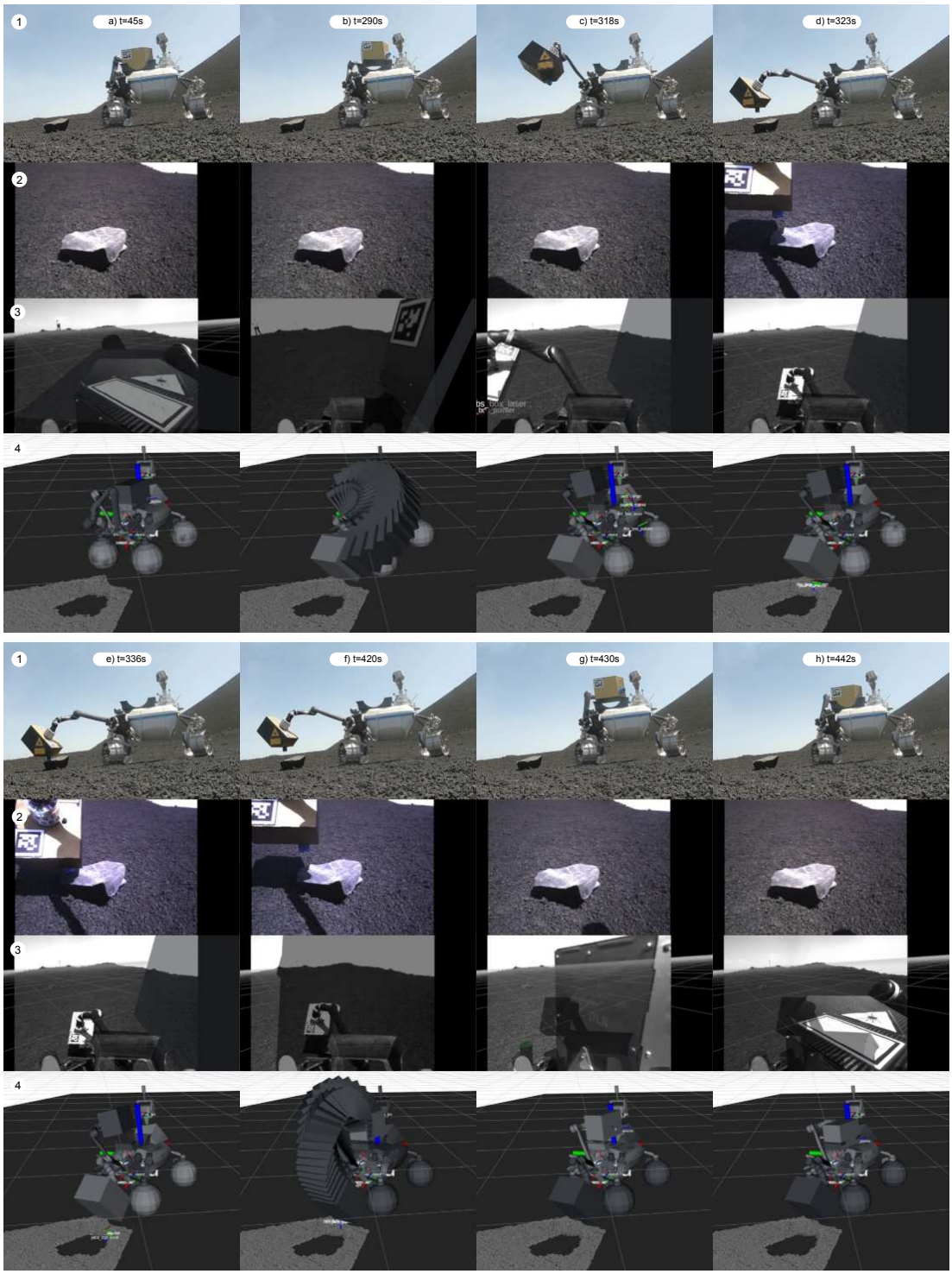

Figure 16: Overview of one manipulation sequence at different time points. Row one (1) shows an external camera view, row two (2) shows the view of the back camera, row three (3) shows the view of the pan-tilt camera and row four (4) shows the internal robot model.

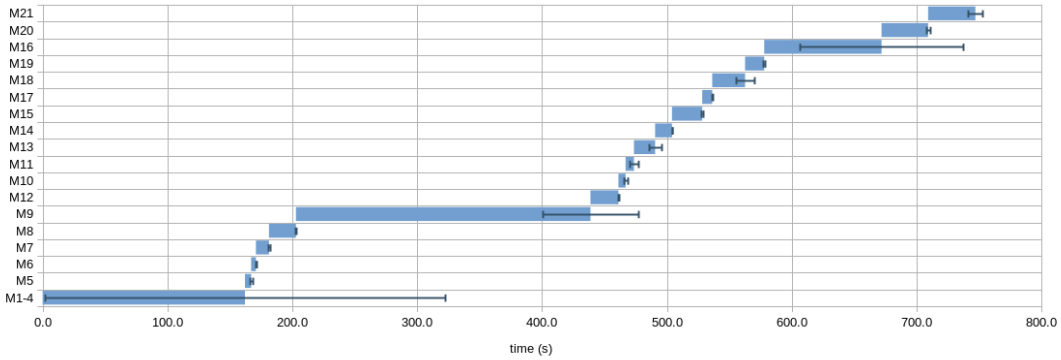

Figure 17: The mean and standard deviation execution time of the manipulation sequence for three executions of the LIBS manipulation sequence. The individual tasks are labeled as indicated in Figure 3.

We evaluated the execution time of the manipulation sequence in Figure 17, which shows the mean and variance of the execution time of the individual steps defined in Figure 3 for three sampling operations, on Mt. Etna. The longest execution time was spent booting and testing the communication to the LIBS instrument after the instrument was docked (M9), which took an average of approximate 236 s. The boot procedure could be further refined from the current prototype to decrease this duration. The second most execution time was spent during the selection of the sample (M1-4), which took an average of approximate 162 s and has a large standard deviation of 160 s. A similar variance can be observed in the download of the sample data (M16), which took an average of 94 s and an has a standard deviation of 65 s. These steps depend on the reaction of mission control to select a sample and to download the measurement data, thus underlie a large variance. Under realistic communication delays these operations would require significantly more time. The remaining, completely autonomous, steps of the sequence took an average of 255 s with a standard deviation of 14 s.

Overall the rover executed the manipulation sequence in an average of 747 s, which translates approximate to a rate of four to five measurements per hour, excluding the time spent driving to sample locations. If manual selection of a particular stone by mission control is not necessary and the download and inspection of the collected data can be done after collecting a set of samples, we extrapolate an average execution time of approximately 520 s, which translates to a rate of seven measurements per hour.

6.3 LIBS Data Acquisition

The acquisition of data with the LIBS instrument on Mt. Etna worked as expected. For the measurements on the experiment site, three different rocks were analyzed on five positions each by using the instrument's scanning mirror. Each position was sampled twenty times.

Figure 18 shows a LIBS-spectrum that was collected from one of the sampled rocks

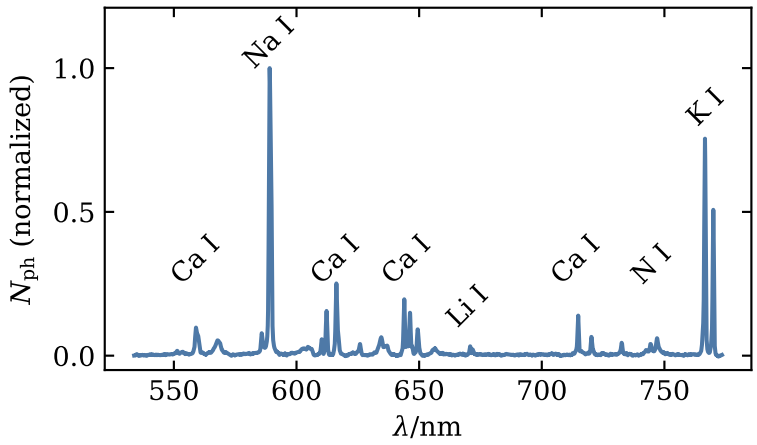

Figure 18: LIBS spectrum from the analog experiment on Mt. Etna. The abscissa shows the wavelength λ and the ordinate shows the photon count N_{ph}.

on the experiment site during the analog experiment campaign. In the presented data, ten subsequent LIBS spectra from the same location were averaged, a dark spectrum was subtracted and the continuum emission was removed. For this, the tools that are also integrated into the LIBS scientific interface GUI were used.

As annotated in Figure 18, the sample contains the major rock-forming elements Calcium (Ca) and Silicon (Si), as well as Sodium (Na), Lithium (Li) and Potassium (K). The Nitrogen (N) emission is a result of the breakdown of ambient air that also contributes to the plasma. A detailed scientific investigation of the acquired data will be part of a future publication. The spectrum has a signal-to-noise ratio of about 14 for the weakest identified emission line (Li I) and is thus suitable for scientific analysis.

7 Discussion

The results show that the prototype LRU rover system can autonomously sample individual rocks in an Moon analog environment with the LIBS instrument. The presented autonomy allows to perform sampling operations in a short amount of time, without supervision from mission control. This increases the data generated during a mission and allows to gather samples in communication denied areas. While we were able to demonstrate this complex behavior on a reasonable prototype, much work remains to qualify the individual hardware and software components for a final space ready system, as those presented in the related work, for example [1][2][3].

During the test campaign we identified different challenges. On the rover system, the manipulator needs to be light, but also be able to manipulate relatively heavy payloads. Since the gravitational force is much higher on Earth than on the target celestial bodies,

the manipulator had to be strained to the torque limits. This increases the complexity of the autonomous software, since the manipulator must execute operations quickly, to not overheat. Designing and implementing a manipulator which can carry the specified load indefinite during test campaigns on Earth, would significantly simplify testing.

Due to the light design of the rover system as well as the manipulator, the system exhibits elasticity in the joints between the main body and the wheels, at the base of the manipulator, and in the manipulator joints. We took major efforts to model these elasticities, calibrate the system to the camera system, and programmed an autonomous calibration routine. Nevertheless, increasing the stiffness in the overall system hardware design would relax the constraints on the model accuracy and increase the robustness of the system.

While we describe the system from a high level autonomy perspective, many challenges lie also within the integration of the system as a whole. To solve the complexity of interfacing the many components on the system, we developed and tested a new continuous integration chain for our software as part of the project.

8 Conclusions

In this contribution we presented a rover prototype which can autonomously deploy an attachable LIBS instrument with a manipulator in a Moon analog context. The modular design in combination with the manipulator allows for flexible use of the instrument. The autonomous capabilities reduce the need for supervision, increasing productivity and allowing the system to gather scientific data in communication denied environments.

We evaluated the rover and instrument prototypes as a proof of concept at an analog site on Mt. Etna, successfully completing autonomous measurements with relevant scientific data. In future work we will refine the technology readiness level of the individual prototypes, improve the interfaces between the individual components and perform a in-depth evaluation of the sampling process at a different test site.

9 Acknowledgments

We gratefully acknowledge the funding provided by the Helmholtz Association, in the strategic future topic ARCHES ZT-0033, and in the sustainability challenge iFOODis KA-HSC-06_iFOODis. We thank our colleagues from the German Aerospace Center (DLR) for their continued support during the preparation as well as during the experiments on Mt. Etna.

References

[1] R. C. Wiens, S. Maurice, B. Barraclough, M. Saccoccio, W. C. Barkley, J. F. Bell, S. Bender, J. Bernardin, D. Blaney, J. Blank, *et al.*, "The chemcam instrument suite

on the mars science laboratory (MSL) rover: Body unit and combined system tests," *Space science reviews*, vol. 170, no. 1, pp. 167–227, 2012.

[2] S. Maurice, R. Wiens, M. Saccoccio, B. Barraclough, O. Gasnault, O. Forni, N. Mangold, D. Baratoux, S. Bender, G. Berger, *et al.*, "The chemcam instrument suite on the mars science laboratory (MSL) rover: Science objectives and mast unit description," *Space science reviews*, vol. 170, no. 1, pp. 95–166, 2012.

[3] S. Maurice, S. M. Clegg, R. C. Wiens, O. Gasnault, W. Rapin, O. Forni, A. Cousin, V. Sautter, N. Mangold, L. Le Deit, *et al.*, "Chemcam activities and discoveries during the nominal mission of the mars science laboratory in gale crater, mars," *Journal of Analytical Atomic Spectrometry*, vol. 31, no. 4, pp. 863–889, 2016.

[4] A. Laxmiprasad, V. S. Raja, S. Menon, A. Goswami, M. Rao, and K. Lohar, "An in situ laser induced breakdown spectroscope (LIBS) for chandrayaan-2 rover: Ablation kinetics and emissivity estimations," *Advances in Space Research*, vol. 52, no. 2, pp. 332–341, 2013.

[5] R. C. Wiens, S. Maurice, S. H. Robinson, A. E. Nelson, P. Cais, P. Bernardi, R. T. Newell, S. Clegg, S. K. Sharma, S. Storms, *et al.*, "The supercam instrument suite on the nasa mars 2020 rover: body unit and combined system tests," *Space Science Reviews*, vol. 217, no. 1, pp. 1–87, 2021.

[6] S. Maurice, R. C. Wiens, P. Bernardi, P. Caïs, S. Robinson, T. Nelson, O. Gasnault, J.-M. Reess, M. Deleuze, F. Rull, *et al.*, "The supercam instrument suite on the mars 2020 rover: science objectives and mast-unit description," *Space Science Reviews*, vol. 217, no. 3, pp. 1–108, 2021.

[7] M. J. Schuster, S. G. Brunner, K. Bussmann, S. Büttner, A. Dömel, M. Hellerer, H. Lehner, P. Lehner, O. Porges, J. Reill, *et al.*, "Towards autonomous planetary exploration," *Journal of Intelligent & Robotic Systems*, vol. 93, no. 3, pp. 461–494, 2019.

[8] I. A. Nesnas, L. M. Fesq, and R. A. Volpe, "Autonomy for space robots: Past, present, and future," *Current Robotics Reports*, vol. 2, no. 3, pp. 251–263, 2021.

[9] M. J. Schuster, M. G. Müller, S. G. Brunner, H. Lehner, P. Lehner, R. Sakagami, A. Dömel, L. Meyer, B. Vodermayer, R. Giubilato, *et al.*, "The ARCHES space-analogue demonstration mission: Towards heterogeneous teams of autonomous robots for collaborative scientific sampling in planetary exploration," *IEEE Robotics and Automation Letters*, vol. 5, no. 4, pp. 5315–5322, 2020.

[10] S. Hayati, R. Volpe, P. Backes, J. Balaram, R. Welch, R. Ivlev, G. Tharp, S. Peters, T. Ohm, R. Petras, *et al.*, "The rocky 7 rover: a mars sciencecraft prototype," in *Proc. IEEE Int. Conf. Robotics and Automation (ICRA)*, vol. 3, pp. 2458–2464, IEEE, 1997.

[11] E. Baumgartner, R. Bonitz, J. Melko, L. Shiraishi, and P. Chris Leger, "The mars exploration rover instrument positioning system," in *Proc. 2005 IEEE Aerospace Conf.*, pp. 1–19, 2005.

[12] R. Rieder, R. Gellert, J. Brückner, G. Klingelhöfer, G. Dreibus, A. Yen, and S. Squyres, "The new athena alpha particle x-ray spectrometer for the mars exploration rovers," *Journal of Geophysical Research: Planets*, vol. 108, no. E12, 2003.

[13] R. C. Anderson, L. Jandura, A. Okon, D. Sunshine, C. Roumeliotis, L. Beegle, J. Hurowitz, B. Kennedy, D. Limonadi, S. McCloskey, *et al.*, "Collecting samples in gale crater, mars; an overview of the mars science laboratory sample acquisition, sample processing and handling system," *Space science reviews*, vol. 170, no. 1, pp. 57–75, 2012.

[14] M. Robinson, C. Collins, P. Leger, J. Carsten, V. Tompkins, F. Hartman, and J. Yen, "In-situ operations and planning for the mars science laboratory robotic arm: The first 200 sols," in *8th Int. Conf. on System of Systems Engineering*, pp. 153–158, IEEE, 2013.

[15] V. Verma, T. Estlin, G. Doran, D. Gaines, R. Francis, P. Romano, C. Skeggs, and R. Castano, "Results from the first four years of aegis autonomous target-ing for chemcam on mars science laboratory and new capability planned for supercam on mars 2020 rover," 2020.

[16] V. Verma, J. Huang, P. Bailey, J. Carsten, and D. Klein, "Perseverance rover collision model for a range of autonomous behaviors," in *2022 IEEE Aerospace Conf.*, pp. 1–18, IEEE, 2022.

[17] T. M. Roehr, F. Cordes, and F. Kirchner, "Reconfigurable integrated multirobot exploration system (rimres): Heterogeneous modular reconfigurable robots for space exploration," *Journal of Field Robotics*, vol. 1, no. 31, pp. 3–34, 2013.

[18] M. Jankovic, W. Brinkmann, S. Bartsch, R. Palazzetti, and X. Yan, "Concepts of active payload modules and end-effectors suitable for standard interface for robotic manipulation of payloads in future space missions (sirom) interface," in *2018 IEEE Aerospace Conf.*, pp. 1–15, IEEE, 2018.

[19] A. Wedler, M. Vayugundla, H. Lehner, P. Lehner, M. J. Schuster, S. G. Brunner, W. Stürzl, A. Dömel, H. Gmeiner, B. Vodermayer, *et al.*, "First Results of the ROBEX Analogue Mission Campaign: Robotic Deployment of Seismic Networks for Future Lunar Missions," in *Proceedings of the International Astronautical Congress*, International Astronautical Federation, 2017.

[20] P. Lehner, S. Brunner, A. Dömel, H. Gmeiner, S. Riedel, B. Vodermayer, and A. Wedler, "Mobile manipulation for planetary exploration," in *2018 IEEE Aerospace Conf.*, pp. 1–11, IEEE, 2018.

[21] W. Xu, X. Liu, Z. Yan, L. Li, Z. Zhang, Y. Kuang, H. Jiang, H. Yu, F. Yang, C. Liu, *et al.*, "The marscode instrument suite on the mars rover of china's tianwen-1 mission," *Space Science Reviews*, vol. 217, no. 5, pp. 1–58, 2021.

[22] J. Lasue, R. Wiens, S. Clegg, D. Vaniman, K. Joy, S. Humphries, A. Mezzacappa, N. Melikechi, R. McInroy, and S. Bender, "Remote laser-induced breakdown spectroscopy (LIBS) for lunar exploration," *Journal of Geophysical Research: Planets*, vol. 117, no. E1, 2012.

[23] S. Kubitza, S. Schröder, E. Dietz, S. Frohmann, P. B. Hansen, K. Rammelkamp, D. S. Vogt, M. Gensch, and H.-W. Hübers, "Detecting sulfur on the moon: The potential of vacuum ultraviolet laser-induced breakdown spectroscopy," *Spectrochimica Acta Part B: Atomic Spectroscopy*, vol. 174, p. 105990, 2020.

[24] A. Wedler, B. Rebele, J. Reill, M. Suppa, H. Hirschmüller, C. Brand, M. Schuster, B. Vodermayer, H. Gmeiner, A. Maier, *et al.*, "LRU-lightweight rover unit," in *Proc. 13th Symposium on Advanced Space Technologies in Robotics and Automation (ASTRA)*, 2015.

[25] A. F. Prince, B. Vodermayer, B. Pleintinger, A. Kolb, Emanuel, Staudinger, E. Dietz, S. Schröder, S. Frohmann, F. Seel, and A. Wedler, "Design and implementation of a modular mechatronics infrastructure for robotic planetary exploration assets," in *Proc. of the Int. Astronautical Congress*, IAC, 2021.

[26] S. G. Brunner, F. Steinmetz, R. Belder, and A. Dömel, "RAFCON: A graphical tool for engineering complex, robotic tasks," in *Proc. IEEE/RSJ Int. Conf. Intelligent Robots and Systems (IROS)*, pp. 3283–3290, October 2016.

[27] M. Durner, W. Boerdijk, M. Sundermeyer, W. Friedl, Z.-C. Márton, and R. Triebel, "Unknown Object Segmentation from Stereo Images," in *Proc. 2021 IEEE/RSJ Int. Conf. Intelligent Robots and Systems (IROS)*, pp. 4823–4830, Sept. 2021.

[28] W. Boerdijk, M. G. Muller, M. Durner, M. Sundermeyer, W. Friedl, A. Gawel, W. Stürzl, Z.-C. Marton, R. Siegwart, and R. Triebel, "Rock Instance Segmentation from Synthetic Images for Planetary Exploration Missions," p. 3, 2021.

[29] S. M. Milkovich, K. M. Stack, V. Z. Sun, K. Maxwell, R. Kronyak, S. L. Schnadt, K. Steadman, and N. Spanovich, "Balancing predictive and reactive science planning for mars 2020 perseverance," in *Proc. 2022 IEEE Aerospace Conference*, pp. 1–12, 2022.

[30] H. Hirschmuller, "Accurate and Efficient Stereo Processing by Semi-Global Matching and Mutual Information," in *Proc. IEEE Computer Society Conf. on Computer Vision and Pattern Recognition (CVPR)*, vol. 2, pp. 807–814, IEEE, 2005.

[31] A. Hornung, K. M. Wurm, M. Bennewitz, C. Stachniss, and W. Burgard, "OctoMap: An efficient probabilistic 3D mapping framework based on octrees," *Autonomous Robots*, vol. 34, pp. 189–206, Apr. 2013.

[32] S. M. LaValle, "Rapidly exploring dense trees," *Planning Algorithms*, pp. 228–237, 2004.

[33] D. Berenson, S. S. Srinivasa, and J. Kuffner, "Task space regions: A framework for pose-constrained manipulation planning," *The Int. Journal of Robotics Research*, vol. 30, no. 12, pp. 1435–1460, 2011.

[34] R. Geraerts and M. H. Overmars, "Creating high-quality paths for motion planning," *The Int. Journal of Robotics Research*, vol. 26, no. 8, pp. 845–863, 2007.

[35] P. Lehner and A. Albu-Schäffer, "The repetition roadmap for repetitive constrained motion planning," *IEEE Robotics and Automation Letters*, vol. 3, no. 4, pp. 3884–3891, 2018.

[36] N. Hogan, "Impedance Control: An Approach to Manipulation: Part I - Theory, Part II - Implementation, Part III - Applications," *Journal of Dynamic Systems, Measurement, and Control*, vol. 107, pp. 1–24, Mar. 1985.

[37] A. Albu-Schäffer, C. Ott, and G. Hirzinger, "A Unified Passivity-based Control Framework for Position, Torque and Impedance Control of Flexible Joint Robots," *Int. Journal of Robotics Research*, vol. 27, pp. 23–39, Jan. 2007.

[38] C. Ott, A. Albu-Schäffer, A. Kugi, and G. Hirzinger, "On the Passivity-Based Impedance Control of Flexible Joint Robots," *IEEE Transactions on Robotics*, vol. 24, pp. 416–429, Apr. 2008.

[39] P. B. Hansen, *Modeling of LIBS Spectra Obtained in Martian Atmospheric Conditions*. PhD thesis, Humboldt-Universität zu Berlin, 2021.

[40] L. Preston, M. Grady, and S. Barber, "CAFE – Concepts for Activities in the Field for Exploration – TN2: the catalogue of planetary analogues," Dec. 2012.

[41] V. Ciarletti, S. Clifford, A. J. Vieau, B. Lustrement, R. Hassen Khodja, and P. Cais, "Results from the first field tests of the WISDOM GPR (2018 ExoMars mission)," in *42nd Lunar and Planetary Science Conference*, (Houston), p. Abstract #2613, Lunar and Planetary Institute, 2011.